Small Error Dynamics and the Predictability of Atmospheric Flows

BRIAN F. FARRELL

Department of Earth and Planetary Sciences, Harvard University, Cambridge, Massachusetts

(Manuscript received 23 October 1989, in final form 19 April 1990)

ABSTRACT

Forecast reliability is known to be highly variable and this variability can be traced in part to differences in the innate predictability of atmospheric flow regimes. These differences in turn have traditionally been ascribed to variation in the growth rate of exponential instabilities supported by the flow. More recently, drawing on modern dynamical systems theory, the asymptotic divergence of trajectories in phase space of the nonlinear equations of motion has been cited to explain the observed loss of predictability. In this report it is shown that increase in error on synoptic forecast time scales is controlled by rapidly growing perturbations that are not of normal mode form. It is further noted that unpredictable regimes are not necessarily associated with larger exponential growth rates than are relatively more predictable regimes. Moreover, model problems illustrating baroclinic and barotropic dynamics suggest that asymptotic measures of divergence in phase space, while applicable in the limit of infinite time, may not be appropriate over time intervals addressed by present synoptic forecast.

1. Introduction

Richardson's vision of predicting the weather by integrating the equations of motion (Richardson 1922) remains a central preoccupation of meteorology today; and the discipline could not hope for a more objective measure of its progress than is provided by the daily forecast verification. Despite the availability of a vast synoptic dataset augmented by surface, airplane, and satellite observations and use of the most powerful computers, the goal of providing reliable forecast beyond a few days has proved elusive. In an effort to comprehend the apparent difficulty of this problem studies have been conducted beginning with the first modern NWP efforts to assess the limits of predictability (Thompson 1957). With the exception of Lorenz (1969), these have concentrated on the sensitivity of models to perturbations using direct integration of initially nearby states (Charney et al. 1966; Smagorinsky 1969; Lorenz 1982; Dalcher and Kalney 1987; Chen 1989). These studies probe behavior of models directly and are augmented in some cases by comparison of model results with observations. Lorenz's search for analog states in observations provided a direct measure of predictability, unfortunately no close analogues were found. Results of these studies can be summarized by the error equation:

$$\frac{dE}{dt} = \alpha E - \gamma E^2 \qquad (1.1)$$

in which E is some measure of error such as the rms 500 hPa deviation between forecasts, α is an exponential error growth rate, and γ enforces saturation at the variance of uncorrelated realizations. Identification of α with exponential instability is plausible because values of the order of a few days for doubling are found that compare approximately with the growth rate of unstable waves although there is fairly wide variation in both these quantities. However, such a simple explanation is not likely to be complete because it is known that the error growth is distributed irregularly in space and time (Lorenz 1965; Hoffman and Kalnay 1983) and does not correlate with instability measures (Kallen and Huang 1988; Palmer 1988). Moreover, the doubling time is an integral average quantity that is not easily associated with what are often highly localized variations in stability measures. Plots of increase in error with time (Hoffman and Kalnay 1983; Chen 1989) tend to rise smoothly to saturation suggesting that alternative two-parameter functions may serve as well as (1.1).

In the study referred to above, Palmer (1988) finds predictability of the ECMWF forecast model varies with the flow regime, and when unpredictable regimes are isolated they have enhanced response to perturbations but there is no corresponding enhancement of exponential instability. This finding is at least compatible with results on the excitation of baroclinic flows in which perturbation development is found even in the absence of exponential instability (Farrell 1985, 1989).

The predictability problem is intrinsically linear in its early stages. Nonlinearity affects the evolving basic state that is perturbed and ultimately it also affects the

Corresponding author address: Prof. Brian Farrell, Dept. of Earth & Planetary Sciences, Harvard University, Pierce Hall, 29 Oxford St, Cambridge, MA 02138.

saturation of the perturbation growth. Yet, for sufficiently small perturbations there is an interval in which the tangent linear equations are valid. While progress being made in nonlinear dynamics offers hope for a complete theory of predictability including the saturation stage, well-known methods suffice for understanding the linear interval. In this work, linear small error theory is applied to the study of predictability. A simple baroclinic shear model and a barotropic channel model with a localized jet are used as examples.

2. Linear theory of predictability

The dynamics of small errors that forms the theoretical basis of this work was introduced into the study of predictability by Lorenz (1965) and used recently by Lacarra and Talagrand (1988) [see also Dutton and Wells (1984)]. Consider the state of the atmosphere indicated by a point in an appropriate phase space. Nonlinear equations of motion govern the trajectory of the system from an initial time t_0 to a later time t_1, but for sufficiently small perturbations of the initial state at t_0 and for a correspondingly restricted interval of time $\tau = t_1 - t_0$ the equations governing perturbations are linear; the tangent linear system linearized about the unperturbed trajectory.

Explicitly, the nonlinear equation:

$$\frac{d\Psi}{dt} = \mathbf{F}(\Psi) \tag{2.1}$$

with solution $\Psi_0(t)$ is associated with the linear error equation:

$$\frac{d\psi}{dt} = \mathbf{L}\psi, \tag{2.2}$$

in which $\mathbf{L} \equiv (\partial \mathbf{F}/\partial \Psi)(\Psi_0(t))$ is in general a function of time. In the present study Ψ_0 is restricted to stationary solutions making the error equation autonomous and also a discretization is performed so that $\mathbf{L}$ can be written as a matrix and ψ as a vector. The resolvent of (2.2) at $t = \tau$ is denoted by $\mathbf{A}_\tau$ so that $\psi(\tau) = \mathbf{A}_\tau\psi(0)$. A measure of the magnitude of ψ that distinguishes between large and small errors requires definition of a norm $|\psi| = (\psi^*\mathbf{B}\psi)^{1/2}$ where $\mathbf{B}$ denotes a positive definite quadratic form and a superscript star denotes the Hermitian transpose. In a related study of optimal excitation, Farrell (1988, 1989) found results were sensitive to the choice of norm, and the reasons for this are of interest. Traditionally $\mathbf{B} = \mathbf{I}$ is chosen, $\mathbf{I}$ denoting the identity matrix. There are drawbacks to this choice of the rms streamfunction deviation to measure perturbations: in baroclinic problems it emphasizes waves that propagate from lower regions where the density is high into the stratosphere growing primarily as a result of the exponential density stratification. In both baroclinic and barotropic dynamics the rms streamfunction norm permits disturbances with large localized velocity to be considered small perturbations because derivatives of the streamfunction, corresponding to velocity, do not enter directly in the definition of the norm. Although previous work on the predictability problem has tended to use a measure based on the rms streamfunction, often height of the 500 hPa surface, in this study $\mathbf{B}$ is chosen to be the operator which, in the volume integral, returns total perturbation energy.

Error dynamics can be viewed as the evolution along the solution trajectory of the initial error, spherical in the energy norm, into an ellipse in that norm according to:

$$\phi_i^*[\mathbf{A}_\tau^*\mathbf{B}\mathbf{A}_\tau]\phi_i = \lambda_i\phi_i^*\mathbf{B}\phi_i. \tag{2.3}$$

Axes of the error ellipse at time τ are proportional to $\lambda_i^{1/2}$ and the corresponding eigenvectors ϕ_i are a linearly independent $\mathbf{B}$ orthogonal set that span the space of perturbations and can be ordered by magnitude, the largest λ being the factor by which the energy of the optimal ϕ increases over the time interval τ. The ϕ_i are a linearly independent set of functions into which the energy of an initial perturbation is partitioned by $\mathbf{B}$ projection. The spectrum λ_i provides information needed to understand predictability in the linear regime, for instance the volume of the error ellipse at $t = \tau$ is proportional to $\prod_{i=1}^{N} \lambda_i^{1/2}$. This volume is constant in the absence of dissipation but becomes more contracting with greater damping. Values of $\lambda_i > 1$ are associated with perturbations that increase in energy, while perturbations with $\lambda_i < 1$ decay. It is of interest to know the size of the subspace of growing perturbations and whether it is dominated by a few disturbances. The optimal excitation, which is associated with the largest eigenvalue, is the most amplifying disturbance and it will turn out not to have the form of an exponential normal mode. The structure into which this perturbation evolves at time τ is the preferred response of the system on this time scale, its structure is also of interest. The sum $(1/N)\sum_1^N \lambda_i$ is the factor by which perturbation variance increases under the assumption that every perturbation is excited equally. Even if error ellipse volume is contracting, some λ_i's may be large enough so that total variance increases. By solving for the spectrum on the interval $0 < \tau < \tau_0$, an assessment of the growth of error for an ensemble excitation can be found and compared with the prediction of a constant exponential growth as in the small error limit of (1.1).

3. Predictability of baroclinic shear flow

Although the theoretical basis for understanding predictability of small errors is general and applies to any set of dynamical equations, it is useful to restrict a preliminary investigation of its implication to simplified dynamics and well known examples. Many studies in the past addressed global predictability, often with a full GCM. While those results are directly ap-

plicable to the NWP forecast problem, the intricacies of highly coupled 3D dynamics, often including microphysics, complicates interpretation. The first example studied here is the quasi-geostrophic baroclinic shear problem. The physical situation being modeled is baroclinic development on time scales appropriate to synoptic forecast such as an event of cyclogenesis.

Assuming constant density scale height and including the beta effect the nondimensional perturbation quasi-geostrophic potential vorticity equation for the scaled streamfunction:

$$\psi = \hat{\psi}(\tilde{z}, \tilde{t}) \frac{e^{\tilde{z}/2}}{\sqrt{\epsilon}} e^{i\tilde{k}\tilde{x}} \cos(\tilde{l}\tilde{y}) \tag{3.1}$$

is:

$$\left(\frac{\partial}{\partial \tilde{t}} + i\tilde{k}\tilde{U}\right)\left[\hat{\psi}_{\tilde{z}\tilde{z}} - \left(\tilde{S}^2 - \tilde{S}_{\tilde{z}} + \frac{\tilde{\alpha}^2}{\epsilon}\right)\hat{\psi}\right] + i\tilde{k}\left(\frac{\tilde{\beta}}{\epsilon} + 2\tilde{S} - \tilde{U}_{\tilde{z}\tilde{z}}\right)\hat{\psi} = 0. \tag{3.2}$$

Boundary conditions include Ekman convergence at the lower boundary:

$$\frac{\partial}{\partial \tilde{t}}(\hat{\psi}_{\tilde{z}} + \tilde{S}\hat{\psi}) - i\tilde{k}(\tilde{U}_{\tilde{z}} - \tilde{\Gamma})\hat{\psi} = 0, \quad \tilde{z} = 0. \tag{3.3a}$$

$$\frac{\partial}{\partial \tilde{t}}(\hat{\psi}_{\tilde{z}} + \tilde{S}\hat{\psi}) - i\tilde{k}\tilde{U}_{\tilde{z}}\hat{\psi} = 0, \quad \tilde{z} = 2. \tag{3.3b}$$

The first meridional mode with $\hat{\psi} = 0$ at $y = \pm(\pi/2\tilde{l})$ is assumed, and the nondimensionalizations $\tilde{t} = t\Lambda\sqrt{\epsilon_0}$, $\tilde{k} = kH/\sqrt{\epsilon_0}$, $\tilde{z} = z/H$ are made. We define the total wavenumber $\tilde{\alpha} = \sqrt{\tilde{k}^2 + \tilde{l}^2}$, and the square ratio of the Coriolis parameter to the Brunt–Väisälä frequency $\hat{\epsilon} = f_0^2/N^2$; then we scale $\hat{\epsilon}$ by a characteristic value, $\epsilon_0 = f_0^2/N_0^2$, so that $\epsilon = \hat{\epsilon}/\epsilon_0$. The problem is characterized by the nondimensional beta parameter $\tilde{\beta} = \beta H/\Lambda\epsilon_0$, the Ekman parameter:

$$\tilde{\Gamma} = \frac{iN}{\Lambda H}\left(\frac{\nu}{2f_0}\right)^{1/2}\frac{\tilde{\alpha}^2}{\tilde{k}}, \tag{3.4}$$

and the stability parameter:

$$\tilde{S} = -\frac{1}{2}\left(\frac{\epsilon_{\tilde{z}}}{\epsilon} - 1\right) \tag{3.5}$$

where ν is the vertical eddy viscosity coefficient and Λ is a mean value of the shear.

Tildes are dropped in sequel.

We choose parameter values appropriate to the midlatitude troposphere: $f_0 = 10^{-4}\ \mathrm{s}^{-1}$, $N = 10^{-2}\ \mathrm{s}^{-1}$, $H = 10$ km $\Lambda = 3\ \mathrm{m\ s^{-1}\ km^{-1}}$, and $\beta = 1.6 \times 10^{-11}\ \mathrm{m^{-1}\ s^{-1}}$. This results in $\beta = 0.53$. The meridional wavenumber $l = 2.0$ corresponds to a 3100 km wavelength typical of midlatitude cyclogenesis. With these values, a unit of nondimensional time is 9.3 h.

This problem, together with its boundary conditions, can be written in matrix operator notation using centered differences on N points and assuming the solution form $\hat{\psi}_j = \hat{E}_j e^{(ikx+\omega_j t)}\cos(ly)$ as:

$$\mathbf{L}\hat{\mathbf{E}}_j = \omega_j \hat{\mathbf{E}}_j, \tag{3.6}$$

where $\hat{\mathbf{E}}_j$ denotes the j'th of N eigenvectors of $\mathbf{L}$.

The vertical structure of the physical streamfunction modes is:

$$\mathbf{E}_j = \mathbf{P}\hat{\mathbf{E}}_j \tag{3.7}$$

where,

$$\mathbf{P} \equiv \frac{e^{z_m/2}}{\sqrt{\epsilon(z_m)}}\delta_{mn}. \tag{3.8}$$

Assuming a fixed wavenumber k, the evolution in time of an initial physical perturbation $\psi(0)e^{ikx}\cos(ly)$ can be expressed as:

$$\psi(\tau) = \mathbf{A}_\tau \psi(0) \tag{3.9}$$

where $\mathbf{A}_\tau$ is the resolvent. Using $\mathbf{E}$, the matrix having the physical eigenvectors as columns, and $\Lambda_\tau \equiv \delta_{mn}e^{(ikx+\omega_m t)}$,

$$\mathbf{A}_\tau = \mathbf{E}\Lambda_\tau\mathbf{E}^{-1}. \tag{3.10}$$

Area average energy is given by $\bar{K} = \psi^*\mathbf{B}\psi$ with:

$$\mathbf{B} \equiv \frac{\rho(0)}{8}[\alpha^2\mathbf{D} + (\mathbf{P}^{-1}\Delta)^*(\mathbf{P}^{-1}\Delta)], \tag{3.11}$$

where $\mathbf{D} \equiv e^{-z_m}\delta_{mn}$ and Δ denotes the finite difference z derivative operator.

Zonal wind and static stability distribution are chosen to model the troposphere and lower stratosphere with zonal wind approaching a constant above one scale height and static stability increasing by a factor of 4 at this simulated tropopause:

$$U(z) = z - (z - 1.5)\left[\frac{1 + \tanh\left(\frac{z - 1.5}{0.5}\right)}{2}\right] \tag{3.12a}$$

$$\epsilon^{-1}(z) = 1 + 3\left[\frac{1 + \tanh\left(\frac{z - 1.5}{0.15}\right)}{2}\right]. \tag{3.12b}$$

Given this wind and static stability it remains to solve (2.2) for the eigenvalues λ_i and the eigenvectors ϕ_i. The spectrum of excitation for the undamped case with $\tau = 6$ corresponding to 55.8 h is shown in Fig. 1 for $N = 100$. Notice the symmetry of the spectrum indicating that volume in phase space is conserved in this norm. There is one unstable mode in the problem with the indicated growth. Clearly neither the dimension of the space of growing perturbations nor the rate of error growth is well represented by the exponential normal mode.

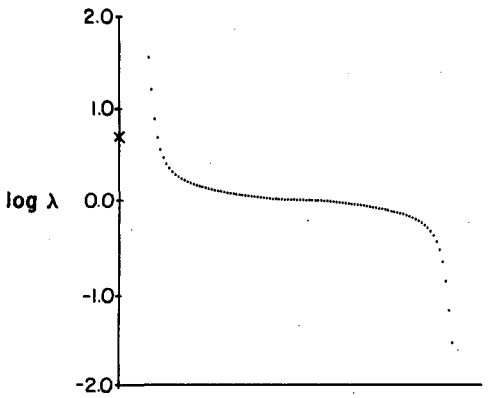

FIG. 1. Spectrum of perturbation energy growth in undamped baroclinic shear flow over six time units corresponding dimensionally to 55.8 h. Growth of the unstable mode would result in the value indicated by the cross. Symmetry of the spectrum is clear in this log plot implying that error ellipse volume is conserved in this energy measure.

Plots of the spectrum similar to Fig. 1 made at lower resolution reveal that the additional modes populate the region of near zero λ_i as resolution is increased, suggesting that $N = 100$ provides sufficient resolution for the values of τ used here. It is possible to assess from a plot such as Fig. 1 a lower bound on the resolution required in a numerical model by examining the structure of the appreciably growing perturbations and choosing a number of collocation points or spectral components necessary to resolve these perturbations.

The spectrum of excitation with $\nu = 10\ \mathrm{m}^2\ \mathrm{s}^{-1}$ ($\Gamma = 0.075$) for which there is no growing exponential normal mode instability is shown in Fig. 2. Error ellipse volume is not conserved. While the number of growing perturbations is nearly equal to the number of those decaying, an estimate of the effective dimension of the error dynamics could be made by counting the appreciably growing perturbations, as there is a fairly robust separation between these and their less favored companions.

Development of the perturbation associated with the largest λ is shown in Fig. 3. This most rapidly growing perturbation resembles the scenario of an upper level disturbance overtaking a lower level depression referred to by Petterssen and Smebye (1971) as type B cyclogenesis.

In both these examples a small number of perturbations dominate the error growth, and a conceptual problem arises if the simplest assumption for calculating the growth of variance is made: equal excitation of the perturbations. The rapidly growing perturbations are represented at low resolution, and as the resolution is increased more slowly, growing and damped modes enter the variance sum, making the apparent predictability an increasing function of resolution. It seems necessary to limit the form of allowed perturbations, perhaps by appeal to observation, so that projection on contracting subspaces is limited in order to make an estimate of variance growth that is convergent with increasing resolution. One rational way of doing this would be to distribute the error according to the observed spatial spectrum of synoptic scale variance. A simpler alternative is suggested by the dominance of error growth by a subset of perturbations: the growth ordered perturbations are partitioned into 1) a lower subset of contracting and slowly growing perturbations with total variance equal to that of the original perturbation and 2) the remaining dominant upper subset responsible for most of the growth in variance. There are six perturbations in the latter for the example in Fig. 3.

Growth of error variance calculated from the largest and the rms of the six largest perturbations is plotted as a function of τ in Fig. 4. Following an initial adjustment, the growth in variance is nearly linear in time rather than exponential as in the error growth model (1.1). Plots of error variance as a function of time obtained from numerical experiments often display a similar interval of linear growth at small error amplitude (Hoffman and Kalnay 1983; Chen 1988). It is important to recognize that the perturbations that dominate the variance differ at each τ, unlike an exponential normal mode dominated growth that would have the structure of the mode at all times.

A centered difference approximation to the growth rate:

$$\sigma = \frac{1}{K}\frac{\Delta K}{\Delta t}$$

is plotted as a function of τ in Fig. 5. Notice that the growth rate is a function of time rather than a constant as would be expected for exponential increase.

It is important to realize that the error growth rate for the $t \to \infty$ asymptotic of this model with realistic damping is zero, as there are no growing exponential normal modes. Asymptotic measures of divergence for

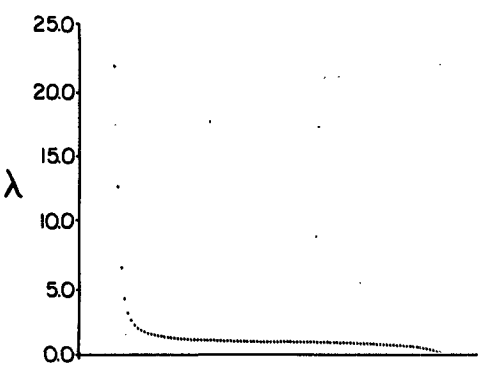

FIG. 2. Spectrum of perturbation energy growth in Ekman damped baroclinic shear flow ($\Gamma = 0.075$) for the energy norm at time $\tau = 6$ corresponding to 55.8 h. Dominance of a few perturbations with large growth can be seen more easily with this linear energy scale. There are no unstable modes.

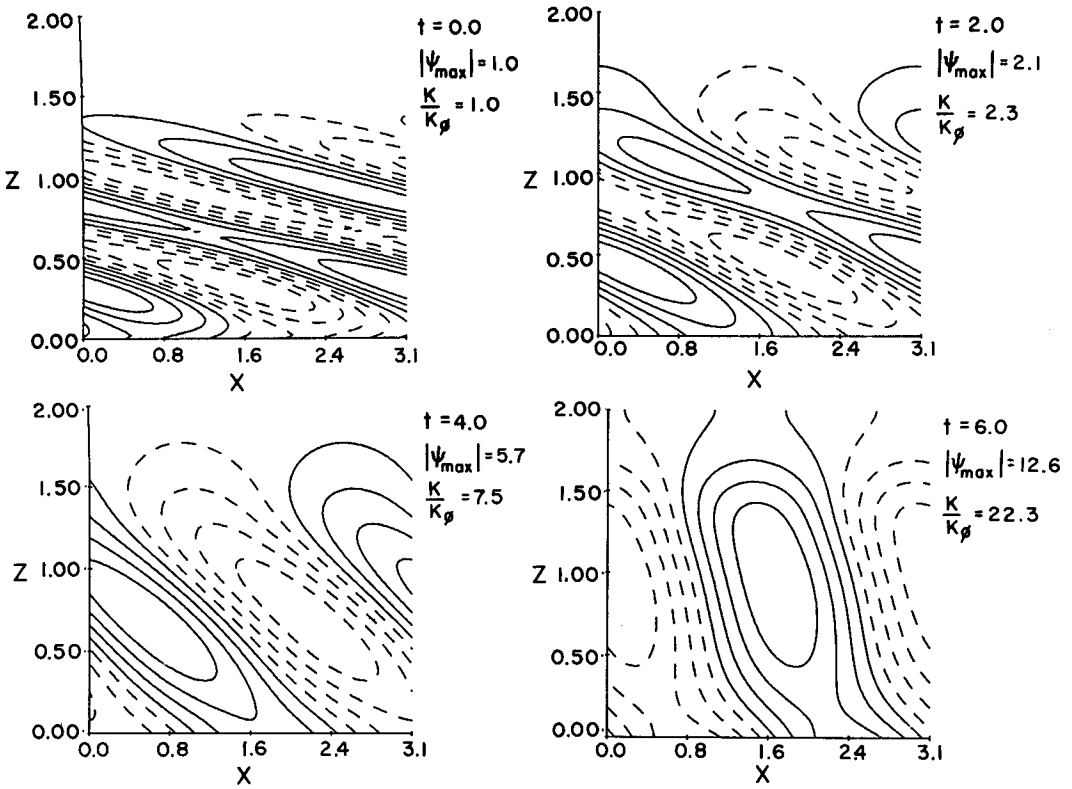

FIG. 3. Development of the perturbation associated with greatest growth in the Ekman damped baroclinic shear problem. Normalized maximum value of perturbation streamfunction and energy are indicated at each time.

nearby states fail in this case to capture essential features of error dynamics on the synoptic forecast time scale.

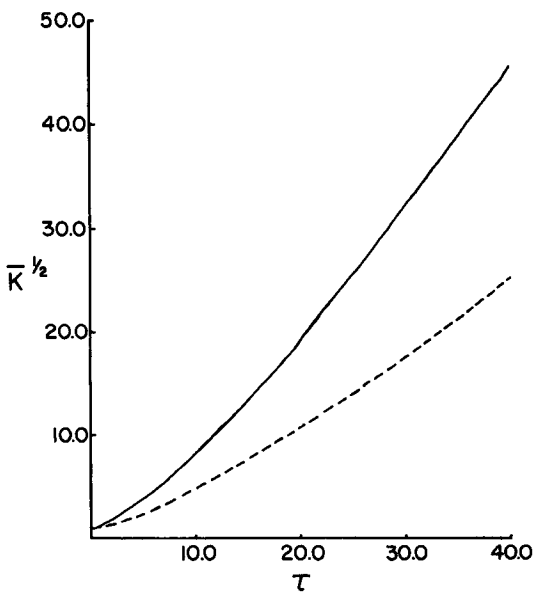

FIG. 4. Error growth as a function of τ in the Ekman damped baroclinic shear problem calculated from the single most rapidly growing perturbation, solid; and the rms growth of the six fastest growing perturbations, dashed.

Consider whether variance on the "slow manifold" (Leith 1980) of synoptic scale motions is primarily externally forced or internally generated. This question is closely related to the problem of transition from ordered to turbulent flow and the dynamics maintaining a turbulent state. It is clear from both the above example and the next example that perturbation variance can be initiated and maintained by amplification of perturbations and that stochastic disturbances grow

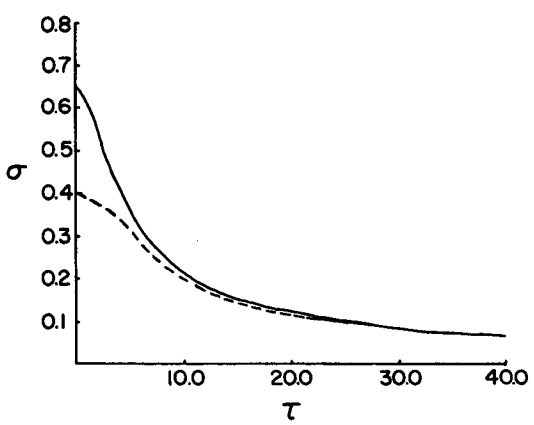

FIG. 5. Instantaneous growth rate as a function of τ for the baroclinic shear flow with Ekman damping, single most rapidly growing perturbation, solid; rms growth of the six fastest growing perturbations, dashed.

under the fairly general circumstance that perturbations not be predominantly restricted to the contracting subspace. In this view the background large scale flow is thought of as an amplifier rather than as an unstable oscillator. Maintenance of variance results from wholly exogenous stochastic excitation or, complementarily, from closing the feedback loop connecting the input of the amplifier to its output by a parameterized process of induced excitation organized by the amplifying disburbances. A concrete example of these processes occurs in the atmosphere where surface concentrations of potential vorticity and temperature gradient become involved in cyclogenesis events. These potential vorticity perturbations can often be traced to diabatic processes such as the formation of coastal fronts augmented by production of potential vorticity associated with latent heat release before and during the cyclogenesis. These are examples of external perturbations injecting potential enstrophy onto the slow manifold of approximately quasi-geostrophic synoptic scale dynamics, but these processes are in turn, to some extent, induced by the large scale flow in a manner at least suggestive of a feedback.

4. Predictability of a barotropic jet

The ideas advanced above should be extended to a fully resolved GCM but there are numerous obstacles to this project, not the least of which is the prohibitive computational demands of the technique used here when it is applied to models with many more degrees of freedom. It is possible however to extend the computation to a barotropic jet localized in two dimensions.

The barotropic vorticity equation governs barotropic flow confined by rigid horizontal boundaries and is regarded as applying at some midtropospheric level of nondivergence when used to model atmospheric dynamics. Linearized about a basic state flow Ψ, the equation is:

$$\frac{\partial}{\partial t}\nabla^2\psi + \left(-\Psi_y\frac{\partial}{\partial x} + \Psi_x\frac{\partial}{\partial y}\right)\nabla^2\psi + (-\psi_y\nabla^2\Psi_x + \psi_x\nabla^2\Psi_y) = 0 \quad (4.1)$$

in which distance is nondimensionalized by the half channel width, and time is nondimensionalized by the ratio L/U where U is the maximum velocity difference across the channel. Typical atmospheric values would be 1000 km and 30 m s^{-1} resulting in 9.3 h per time unit. Periodic boundary conditions are used in x and channel boundaries require ψ = constant along walls at $y = \pm 1$.

A localized jet is defined by

$$\Psi = -\left(0.1y + \frac{\tanh(y\delta(x))}{\tanh(\delta(x))}\right) \quad (4.2)$$

with

$$\delta(x) = 1. + 1.5\left\langle\left\{1 + \cos\left[2\pi\left(\frac{x-2.}{4.}\right)\right]\right\}\Big/2.\right\rangle, \quad 0. < x < 4.$$

The spectrum of error growth in the norm associated with kinetic energy:

$$\bar{K} = \overline{\frac{1}{2}(\psi_y^2 + \psi_x^2)} \quad (4.3)$$

is shown for a total of 450 perturbations resulting from discretization on 30 zonal and 15 meridional grid points in Fig. 6. The subset of growing perturbations is larger in this example and the separation between the dominant and slower growing perturbations is less distinct than in the baroclinic model. Development of the perturbation with the largest growth in six units of nondimensional time corresponding to 56 h is shown in Fig. 7. Orientation of low and high centers in relation to the jet during development corresponds to observations of a process referred to as "trough phasing" in the synoptic literature. Rotation of the troughs from a "positive" toward a "negative" tilt, which continues after the last time shown in the figure, is characteristic of such development.

There is an unstable mode in this undamped model that e-folds in 7.5 nondimensional time units, corresponding to 70 h, and its growth is indicated in Fig. 8. It is worth noting that because the instability is convective rather than absolute, imposition of a Rayleigh damping sponge layer with a time scale of one nondimensional unit confined to the interval $3. < X < 4.$ eliminates the instability. With this damping the decrease in growth of the optimal perturbation at $\tau = 6.$ is only 17%.

Increase in error variance $\bar{K}^{1/2}$ as a function of τ is shown for the most rapidly growing and rms of the dominant 20 perturbations in Fig. 8. A linear increase in rms variance similar to that found in the baroclinic example is found. While the growth of the optimal

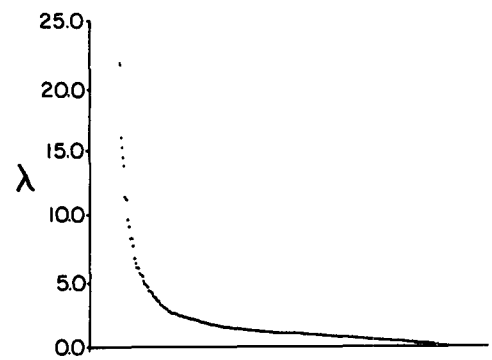

FIG. 6. Spectrum of eigenvalues for the kinetic energy norm in the localized barotropic jet with $\tau = 6$ which corresponds to 55.8 h.

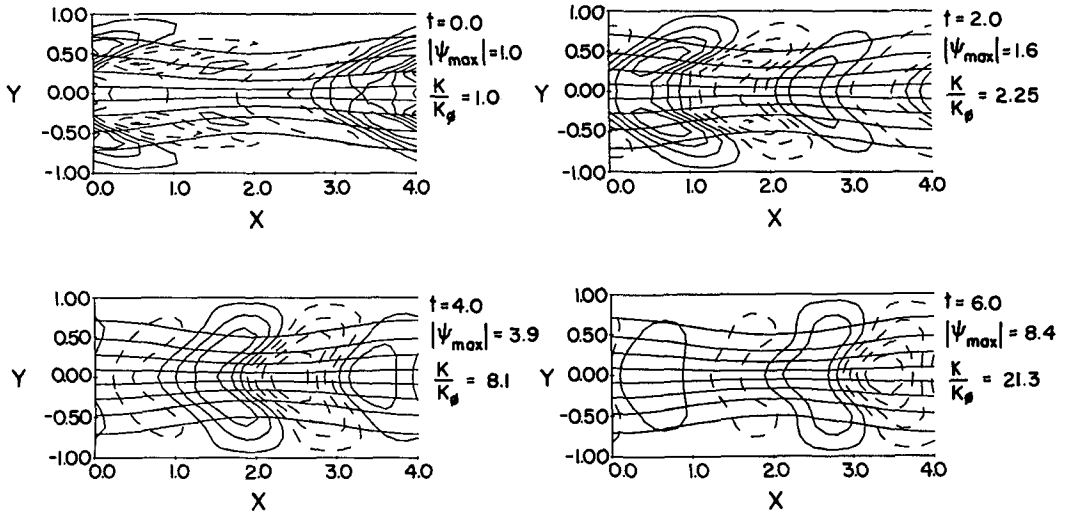

FIG. 7. Development of the perturbation with the greatest growth in energy for the barotropic localized jet at $\tau = 6$, which corresponds to 55.8 h. Streamfunction of the localized jet is superposed. The process of trough phasing and transfer from positive to negative tilt of trough lines during the development can be seen.

perturbation greatly exceeds that of the unstable mode at $\tau = 6.$, even the rms of the first 20 perturbations is larger, indicating that equal excitation of all the perturbations is on average considerably more effective as a means of increasing error than is the direct excitation of the unstable mode.

5. Conclusions

Keeping in mind the limitations of this study, our results for small error growth on stationary states suggest some implications for predictability:

i) Increase of error variance over time scales appropriate to synoptic forecast is determined by the growth of a set of perturbations that are not of exponential normal mode form.

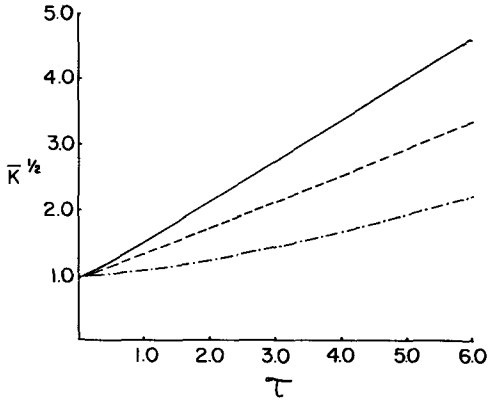

FIG. 8. Error growth as a function of τ calculated using the single most rapidly growing perturbation, solid; rms growth of the twenty fastest growing perturbations, dashed; and the growth of the unstable mode, dash dot.

ii) The set of robustly growing perturbations is much larger than the set of exponential modes but smaller than the set of all perturbations.

iii) An estimate of resolution necessary to accurately model error dynamics over a prescribed time interval can be made by requiring that the perturbations growing appreciably over that interval be resolved.

iv) The most rapidly growing perturbations evolve into structures that can be identified with the preferred responses of the system.

v) Error growth as determined by the rms variance of appreciably growing perturbations is not exponential, and in the examples, increases approximately linearly with time over time scales associated with synoptic forecast.

vi) Asymptotic measures of nearby phase space trajectory divergence, while applicable as $t \to \infty$, fails to capture the relevant error dynamics on synoptic forecast time scales in the models studied here.

vii) Examples demonstrate that provided a straining flow is sufficiently underdamped, there will be systematic amplification of a large subset of imposed broadband disturbances regardless of the flow's exponential stability.

While the theory above can be extended to nonstationary flows in which the resolvent and its adjoint are obtained by integration of the time dependent tangent linear equation and its adjoint equation (Lacarra and Talagrand 1988). The computational burden entailed in isolating the complete spectrum of perturbations appears to be great.

Two major limitations of this study are restriction to small error dynamics that permits the use of linear error equations and the assumption of a stationary basic state that permits these equations to be autonomous.

However, understanding the dynamics of small errors is an important step toward a full theory of predictability. Moreover, while autonomous equations are less rich in dynamics than the time dependent equations resulting from linearization about an evolving trajectory, in a study of an evolving barotropic flow the stationary basic state approximation was found to give accurate results, at least for the most rapidly growing perturbation (Lacarra and Talagrand 1988). The essential reason for this is that the rapidly growing perturbations in the model grow on short time scales compared to the time scale of basic state change, so that ignoring change in the basic state does not severely affect perturbation development.

Acknowledgments. This work was supported by NSF ATM-8912432, NASA through University of Maryland 26929A, and by JVNC NAC00515.

REFERENCES

Charney, J. G., R. G. Fleagle, H. Riehl, V. E. Lally and D. Q. Wark, 1966: The feasibility of a global observation and analysis experiment. *Bull. Amer. Meteor. Soc.*, **47**, 200–220.

Chen, W. Y., 1989: Estimate of dynamical predictability from NMC DERF experiments. *Mon. Wea. Rev.*, **117**, 1227–1236.

Dalcher, A., and E. Kalnay, 1987: Error growth and predictability in operational ECMWF forecasts. *Tellus*, **39A**, 474–491.

Dutton, J. A., and R. Wells, 1984: Topological issues in hydrodynamic predictability. *Predictability of Fluid Motions*, AIP Conf. Proc., **106**, 612 pp.

Farrell, B. F., 1985: Transient growth of damped baroclinic waves. *J. Atmos. Sci.*, **42**, 2718–2727.

——, 1988: Optimal excitation of neutral Rossby waves. *J. Atmos. Sci.*, **45**, 163–172.

——, 1989a: Optimal excitation of baroclinic waves. *J. Atmos. Sci.*, **46**, 1193–1206.

Hoffman, R. N., and E. Kalnay, 1983: Lagged average forecasting. *Tellus*, **35**, 100–118.

Kallen, E., and X. Huang, 1988: The Influence of isolated observations on short-range numerical weather forecasts. *Tellus*, **40A**, 324–336.

Lacarra, J., and O. Talagrand, 1988: Short-range evolution of small perturbations in a barotropic model. *Tellus*, **40A**, 81–95.

Leith, C. F., 1980: Nonlinear normal mode initialization and quasigeostrophic theory. *J. Atmos. Sci.*, **37**, 958–968.

Lorenz, E. N., 1965: A study of the predictability of a 28-variable atmospheric model. *J. Atmos. Sci.*, **17**, 321–333.

——, 1969: Atmospheric predictability as revealed by naturally occurring analogues. *J. Atmos. Sci.*, **26**, 636–646.

——, 1982: Atmospheric predictability experiments with a large numerical model. *Tellus*, **34**, 505–513.

Palmer, T. N., 1988: Medium and extended range predictability and stability of the Pacific/North American mode. *Quart. J. Roy. Meteor. Soc.*, **114**, 691–713.

Petterssen, S., and S. Smebye, 1971: On the development of extratropical cyclones. *Quart. J. Roy. Meteor. Soc.*, **97**, 457–482.

Richardson, L. F., 1922: *Weather Prediction by Numerical Process.* Cambridge University Press, 236 pp.

Smagorinsky, J., 1969: Problems and promises of deterministic extended range forecasting. *Bull. Amer. Meteor. Soc.*, **50**, 286–311.

Thompson, P. D., 1957: Uncertainty of initial state as a factor in the predictability of large scale atmospheric flow patterns. *Tellus*, **9**, 275–295.